journal of the mechanical behavior of biomedical materials 115 (2021) 104252

Contents lists available at ScienceDirect

Journal of the Mechanical Behavior of Biomedical Materials

journal homepage: www.elsevier.com/locate/jmbbm

Research paper

Chondrocytes respond both anabolically and catabolically to impact loading generally considered non-injurious

Stephany Santos [a], Kelsey Richard [b], Melanie C. Fisher [c], Caroline N. Dealy [c,d], David M. Pierce [a,e,*]

[a] Department of Biomedical Engineering, University of Connecticut, Storrs, CT, United States of America
[b] Department of Global Health, University of Connecticut, Storrs, CT, United States of America
[c] Center for Regenerative Medicine and Skeletal Development, Department of Reconstructive Services, University of Connecticut Health Center, Farmington, CT, United States of America
[d] Department of Orthopaedic Surgery, University of Connecticut Health Center, Farmington, CT, United States of America
[e] Department of Mechanical Engineering, University of Connecticut, Storrs, CT, United States of America

ARTICLE INFO

Keywords:
Articular cartilage
Mechanical impact
Metabolism
Progenitor
Ki67
Sox9
EGFR

ABSTRACT

We aimed to determine the longitudinal effects of low-energy (generally considered non-injurious) impact loading on (1) chondrocyte proliferation, (2) chondroprogenitor cell activity, and (3) EGFR signaling. In an *in vitro* study, we assessed 127 full-thickness, cylindrical osteochondral plugs of bovine cartilage undergoing either single, uniaxial unconfined impact loads with energy densities in the range of 1.5–3.2 mJ/mm^3 or no impact (controls). We quantified cell responses at two, 24, 48, and 72 h via immunohistochemical labeling of Ki67, Sox9, and pEGFR antibodies. We compared strain, stress, and impact energy density as predictors for mechanotransductive responses from cells, and fit significant correlations using linear regressions. Our study demonstrates that low-energy mechanical impacts (1.5–3.2 mJ/mm^3) generally stimulate time-dependent anabolic responses in the superficial zone of articular cartilage and catabolic responses in the middle and deep zones. We also found that impact energy density is the most consistent predictor of cell responses to low-energy impact loading. These spatial and temporal changes in chondrocyte behavior result directly from low-energy mechanical impacts, revealing a new level of mechanotransductive sensitivity in chondrocytes not previously appreciated.

1. Introduction

Acute joint trauma, often incurred during accidents or sports injuries, may trigger a cascade of degenerative events that lead to post-traumatic osteoarthritis (OA). OA, the most common chronic joint disease in the world, afflicts over 30 million people in the US alone (Jia et al., 2016). *In-vitro* studies link post-traumatic OA to catabolic changes in articular cartilage following joint injury including increased degradation of collagen and proteoglycan (Setton et al., 1995), decreased synthesis of proteoglycan, switched synthesis from collagen type II to type I (Lahm et al., 2010), and apoptosis of chondrocytes (Chen et al., 2001), among other mechanotransductive responses. Such catabolic changes lead to articular cartilage degeneration and loss of joint function that greatly reduces quality of life, and is a significant cause of morbidity in aging populations (Ryan et al., 2009).

Mechanical loading can trigger catabolic behaviors from chondrocytes. Lee et al. (2005) and Chan et al. (2005) subjected cartilage explants to acute trauma and reported increased expression of genes that cause matrix degradation among other catabolic changes. However, in these experiments the mechanical treatments caused visible macroscale damage to the surface of articular cartilage such that catabolic responses from chondrocytes may manifest as secondary effects of load-induced macroscale damage. We recently found that even low-energy impacts usually considered non-injurious can cause microscale cracks in the network of collagen (microcracks less than the diameter of chondrocyte lacunae (< 30 μm)) (Kaleem et al., 2017). We do not know if mechanical impact that does not induce visible damage to cartilage triggers catabolic or anabolic responses from chondrocytes.

Anabolic responses from chondrocytes, including increased chondrocyte proliferation and matrix synthesis (Shepard et al., 2013), lead to homeostasis and/or growth of articular cartilage. Anabolic (repair) responses may come from either chondrocytes, the mature cells in articular cartilage, or chondroprogenitor cells, multipotent cells that are capable of chondrogenic differentiation (Seol et al., 2012). Interest is growing in the development of mechanically-informed therapeutic

* Correspondence to: University of Connecticut, Departments of Mechanical Engineering/Biomedical Engineering/Mathematics, United States.
E-mail address: dmpierce@engr.uconn.edu (D.M. Pierce).

https://doi.org/10.1016/j.jmbbm.2020.104252
Received 4 January 2020; Received in revised form 25 November 2020; Accepted 3 December 2020
Available online 17 December 2020
1751-6161/

approaches for post-traumatic OA prevention or treatment that would halt catabolic changes in articular cartilage, and/or stimulate anabolic ones (Anderson et al., 2011).

There are no studies investigating the mechanotransductive behavior of chondrocytes or chondroprogenitor cells in response to low-energy impacts generally considered non-injurious. Chondrocytes present mechanotransductive responses to mechanical treatments with strains as low as 6% (Perera et al., 2010). Chondrocytes also respond to fluid-induced stresses as low as 0.02 Pa (Saha and Kohles, 2010). Microcracks in the network of collagen occur after impact treatments to the articular surface resulting in energy densities as low as 1.5 mJ/mm^3 (Kaleem et al., 2017; Santos et al., 2019), but we do not know the corresponding cell responses. Furthermore, which mechanical measures of impact best predict the responses of chondrocytes or chondroprogenitor cells?

In this study, we aimed to determine the longitudinal effects of low-energy impacts generally considered non-injurious on (1) chondrocyte proliferation, (2) chondroprogenitor cell activity, and (3) EGFR signaling. To these ends, we assessed full-thickness, cylindrical osteochondral plugs of bovine cartilage undergoing either single, uniaxial unconfined impact loads with energy densities in the range of 1.5–3.2 mJ/mm^3 (Santos et al., 2019) or no impact (controls). We quantified cell responses at two, 24, 48, and 72 h via immunohistochemical labeling of Ki67, Sox9, and pEGFR. We also compared strain, stress, and impact energy density as predictors for mechanotransductive responses from cells, and fit significant correlations using linear regressions.

2. Materials and methods

2.1. Preparation of specimens

We received full bovine knees from three skeletally mature animals (18–30 months) packed on ice and within 48 h from slaughter (Animal Technologies, Inc., Tyler, TX). We then extracted cylindrical specimens (3 mm diameter, full thickness) from load-bearing and visibly pristine regions on the medial femoral condyles. We removed as much of the subchondral bone as possible while ensuring that the bottom surfaces were visibly parallel to the articular surface and measured the cartilage thicknesses (h_0) using calipers. We immediately immersed specimens in sterile Phosphate Buffered Saline (PBS, pH 7.4) until testing, which occurred less than two hours from extraction.

2.2. Mechanical impact test

We randomly assigned specimens to one of three impact groups (none, 1.5 mJ/mm^3, 3.2 mJ/mm^3), with impact energy density as the independent variable (Santos et al., 2019). We impacted the articular surface of specimens from the 1.5 mJ/mm^3 and 3.2 mJ/mm^3 impact groups in unconfined compression using a custom drop tower with a 12.4 mm diameter flat metal platen (Kaleem et al., 2017; Santos et al., 2019). We measured the acceleration (±49000 m/s^2; 350A14, PCB Piezotronics, Depew, NY) and the force (22.24 kN; 200B05, PCB Piezotronics) at 100,000 Hz (sampling rate) for the full duration of the test. Post-impact, we submerged specimens in PBS at 37°C for at least 1 h prior to subsequent processing. Specimens from the control group rested in PBS for the duration of the test.

2.3. Data analyses

We determined the actual velocity at the moment of impact v_{imp} and the maximum compression of a specimen Δh_{max} for each test by integrating the acceleration data once and twice respectively (Verteramo and Seedhom, 2007; Kaleem et al., 2017). We also determined the maximum force applied to each specimen f_{max} from the measured force data. We then calculated the maximum engineering strain ϵ (−) as $\epsilon = \Delta h_{max}/h_0$ where h_0 is the corresponding reference thickness. Next, we calculated the maximum first Piola–Kirchhoff (nominal) stress P (MPa) as $P = f_{max}/(\pi r_0^2)$ where r_0 is the initial radius of the specimen (1.5 mm). Finally, we calculated the impact energy density E_{imp} or E (mJ/mm^3) as $E = m v_{imp}^2/(2\pi r_0^2 h_0)$ where m is the total drop mass.

2.4. Cell culture and fixation

Immediately after rinsing the specimens in PBS, we fixed the two-hour post-impact specimens from the control ($n = 14$), the 1.5 mJ/mm^3 impact ($n = 9$), and the 3.2 mJ/mm^3 ($n = 9$) impact groups in 4% paraformaldehyde (Sigma, St. Louis, MO) for four days (cf. Fig. 1). We placed the remaining 95 specimens in 1 mL of sterile media comprised of DMEM/F12 (Gibco, Gaithershburg, MD), 50 mg/ml ascorbic-acid-2-phosphate (Sigma), 0.1% bovine serum albumin (Sigma), 10% fetal bovine serum (Atlanta Biologicals, Flowery Branch, GA), 100 units/mL penicillin (Gibco), and 100 μg/mL streptomycin (Gibco) for culture at 37°C and 5% CO_2 for 24, 48, or 72 h post-impact. Once removed from culture, we also fixed these specimens in 4% paraformaldehyde for four days. We then decalcified all specimens using 14% EDTA with NH_4OH for four days at 4°C with rocking. After decalcification, we washed specimens in PBS and dehydrated through a series of solutions increasing in percent ethanol up to 70% ETOH. Finally we paraffin embedded and sectioned specimens (at 8 μm sections) for histology and immunohistochemistry.

2.5. Image-based assessments

We imaged slides with a Nikon Eclipse E800 microscope using 4×/0.20 NA and 20×/0.50 NA objectives, and 1248 × 936 pixel resolution with a pixel size of 1.75 μm. Using the 4× objective, we obtained single images of the full through-thickness cross-section (cartilage and bone) of each specimen for every histological and immunohistochemical stain and time point. Using the 20× objective, we obtained three to five images through the thickness of every specimen stained for immunohistochemistry (spanning from the SZ to the subchondral bone), with 0 – 600 pixels of image overlap.

2.5.1. Histology

We stained sections with 0.1% Safranin O (Sigma) and counterstained with Weigert's Iron Hematoxylin (Poly Scientific, Bay Shore, NY) and 0.02% aqueous Fast Green (Fisher Scientific, Hampton, NH) (Shepard et al., 2013), and imaged the resulting slides. We used these images to qualitatively assess the articular surface integrity and the full-thickness health of the cartilage matrix (Kamekura et al., 2005).

2.5.2. Immunohistochemistry

In a preliminary study we tested the immunolocalization of C3 protein over 72 h. We did not find appreciable cell death and thus we did not continue to test cell viability in this study (See Digital Supplement). We performed immunohistochemical staining as previously described (Shepard et al., 2013). Briefly, we de-paraffinized, rehydrated, and incubated slides with 3% hydrogen peroxide in water for 15 min. We then blocked rabbit anti-bodies using 10% normal goat serum (Vector Laboratories, Burlingame, CA, USA) following standard protocol, and incubated the slides with primary antibodies in blocking buffer overnight at 4°C. In this study we diluted the following primary antibodies to 1:1000: rabbit anti-Ki67 (Abcam, Cambridge, MA, USA); rabbit anti-Sox9 (Abcam); and rabbit anti-pEGFR (Y1092; Abcam). We washed with Tris Buffered Saline (TBS) pH 7.6 containing 0.1% Tween 20 and incubated the slides with 1:200 biotinylated goat anti-rabbit IgG (Vector Laboratories). We then washed again and incubated the slides with Vectastain Elite ABC Reagent (Vector Laboratories) and developed them with DAB Reagent (Vector Laboratories). Finally, we counterstained with Harris' Hematoxylin (Shandon, Cambridge, UK).

To recreate full-thickness cross-sections from the 20× images, we first selected regions with little or no matrix staining, and excluded

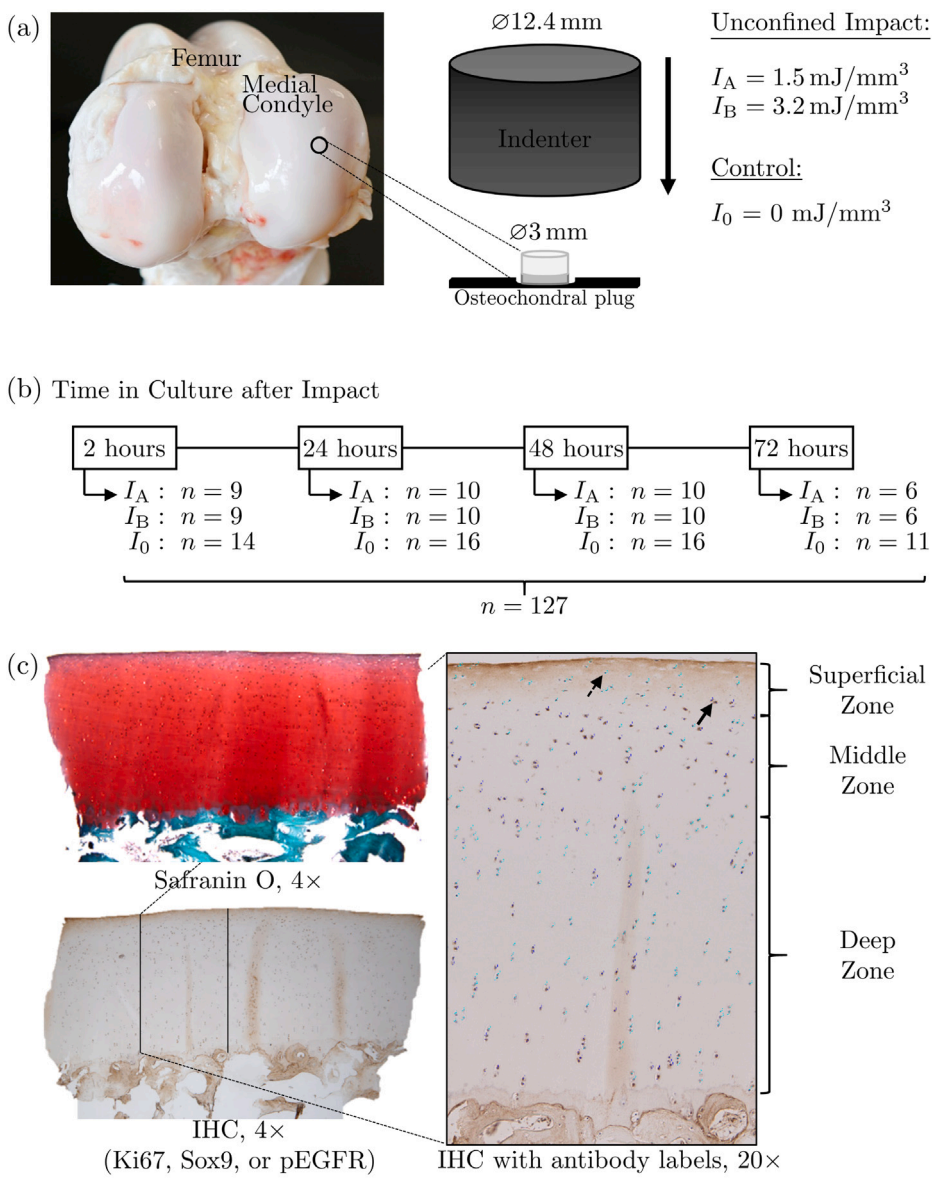

Fig. 1. Graphical representation of the experimental protocol and the treatment groups: (a) specimen extraction and unconfined impact test, (b) time course of specimens in culture by treatment group, (c) representative images from histology (Safranin O/Fast Green in red) and immunohistochemistry with antibody identification. Solid arrows indicate positive antibody expression while dashed arrows indicate negative antibody expression.

specimen edges from the field of view. We then performed image stitching using Fiji's Grid/Collection Stitching Plugin (Preibisch et al., 2009) for ImageJ (National Institutes of Health, Bethesda, MD). Using the resulting full-thickness images, we first determined boundaries for the superficial, middle, and deep zones by assessing lacunae morphology and cellular arrangement (Youn et al., 2006) and defined boundaries between zones as full-width horizontal lines at the average transition height (Pedersen et al., 2013). We also calculated the percent thickness of each zone with respect to total thickness of cartilage. We then quantified both the positive and negative cellular localization of each antibody within each zone, and calculated the percent positive cells within each zone for all images.

2.6. Statistical analyses

We created subsets for each antibody and zone, for a total of nine subsets, and we used these as the basis for subsequent t-tests. Using the Shapiro–Wilk Test we confirmed that our measured percent positive cellular expressions of Ki67, Sox9, and pEGFR were normally distributed. First, we performed separate two-sample t-tests to compare Control vs. Low ($1.5\,mJ/mm^3$) and Control vs. High ($3.2\,mJ/mm^3$) treatment groups to determine if mechanical impacts had significant effects. Then, we used separate two-sample t-tests to compare the means of percent positive cellular expressions of the $1.5\,mJ/mm^3$ and $3.2\,mJ/mm^3$ treatment groups for each corresponding subgroup of equal antibody, time, and zone. We used the pooled t-statistic when groups had equal variances, and the Satterthwaite t-statistic when groups did not have equal variances. We also used separate two-sample t-tests to compare the means of percent positive cellular expressions at every time point. We present our results in tabular form, and also using box plots indicating the medians, the first and third quartiles, and the maximum and minimum values. Second, for significant differences detected by the t-tests, we fit, where possible, separate linear regressions (including R^2 values) to investigate interactions between mechanical stimuli (maximum engineering strain ϵ, maximum first Piola–Kirchhoff (nominal) stress P, and impact energy density E_{imp}) and percent positive cellular expressions. We completed all statistical analyses using SAS 9.4 (SAS Institute Inc., Cary, NC) and with $p < 0.05$ to determine significance.

Table 1
We found statistically significant temporal and zonal differences between the 1.5 mJ/mm^3 and 3.2 mJ/mm^3 impact groups for all antibodies. Summary of p-values from t-tests comparing 1.5 mJ/mm^3 and 3.2 mJ/mm^3 impact groups for the superficial zone (SZ), middle zone (MZ), and deep zone (DZ). We indicate statistical significance ($p < 0.05$) with * and dark gray shading, and marginal statistical significance ($0.05 \leq p < 0.10$) with light gray shading.

Antibody	Zone	2	24	48	72
Ki67	SZ	0.365	0.116	0.697	0.945
	MZ	0.333	**0.016***	0.238	**0.064**
	DZ	0.832	0.447	0.932	**0.031***
Sox9	SZ	**0.043***	0.532	**0.003***	**0.022***
	MZ	0.929	0.144	**0.086**	0.123
	DZ	0.516	0.488	**0.096**	**0.098**
pEGFR	SZ	**0.062**	0.708	0.399	0.206
	MZ	0.163	**0.082**	**0.015***	0.201
	DZ	0.559	0.341	0.237	0.581

In Fig. 1 we summarize the experimental protocol and the treatment groups.

3. Results

We confirmed the overall health and structural integrity of each specimen by analyses of histological images with staining by Safranin O and Fast Green, cf. Fig. 1. We found our low-energy impacts did not induce macroscale damage or visible fissuring at the articular surface. We also qualitatively compared the histological staining of non-impacted control specimens with impacted specimens at the same time points and noted that impacts caused a visible difference in immunohistochemical responses. Using our image-based assessment of the through-thickness zones based on chondrocyte morphology we determined that the SZ, MZ, and DZ within bovine cartilage represented 12 ± 3.9%, 35 ± 17.9%, and 54 ± 17.7% of the overall thickness, respectively.

We determined the reference percent positive cells by antibody and zone using our mechanical controls (no mechanical treatments, only resting in PBS for the equivalent time). In the superficial zone, the control groups presented the following means ± standard deviations (M±SD) for Ki67 (in percent positive cells: 20 ± 20, 40 ± 25, 64 ± 28, 41 ± 31), Sox9 (22 ± 23, 53 ± 24, 41 ± 24, 45 ± 28), and pEGFR (28 ± 20, 34 ± 19, 31 ± 12, 25 ± 17) for 2 h, 24 h, 48 h, and 72 h respectively. In the middle zone, the control groups presented the following M±SD for Ki67 (27 ± 23, 46 ± 20, 52 ± 25, 46 ± 23), Sox9 (38 ± 30, 53 ± 19, 49 ± 17, 55 ± 19), and pEGFR (54 ± 26, 49 ± 15, 54 ± 14, 51 ± 13) for 2 h, 24 h, 48 h, and 72 h respectively. In the deep zone, the control groups presented the following M±SD for Ki67 (40 ± 22, 42 ± 14, 43 ± 21, 39 ± 22), Sox9 (41 ± 26, 41 ± 14, 46 ± 14, 53 ± 11), and pEGFR (56 ± 23, 52 ± 16, 51 ± 11, 44 ± 13) for 2 h, 24 h, 48 h, and 72 h respectively. Comparing against the control group, we found statistically significant differences in the superficial zone — for the antibody Ki67 at 48 h (vs. Low, $p = 0.051$), for Sox9 at 48 h (vs. High, $p = 0.012$), and for pEGFR at 2 h (vs. High, $p = 0.014$); in the middle zone — for Sox9 at 48 h (vs. High, $p = 0.013$) and at 72 h (vs. Low, $p = 0.004$; vs. High, $p = 0.011$), and for pEGFR at 24 h (vs. Low, $p = 0.009$), 48 h (vs. High, $p = 0.036$), and 72 h (vs. High, $p = 0.027$); in the deep zone — for Sox9 at 24 h (vs. Low, $p = 0.021$) and at 72 h (vs. Low, $p = 0.041$), and for pEGFR at 48 h (vs. High, $p = 0.012$).

With this context we present detailed comparisons between low- and high-impact treatments, and look at the subtleties in this range of interest (1.5–3.2 mJ/mm^3). We quantified immuno-labeling (Fig. 2; Appendix A, Fig. 6) and differences between Low- and High-impact-treatment groups (Table 1), and quantified the localization of each antibody by through-thickness zone and time post impact.

3.1. Effects of low-energy impacts on Ki67 and cell proliferation

In the SZ we did not find significant differences in chondrocyte proliferation between impact groups for any time point, as determined by Ki67 labeling. In the MZ at 24 h we found significantly increased ($p = 0.0156$) Ki67 labeling in the 1.5 mJ/mm^3 impact group. We also found a significantly increased ($p = 0.0312$) Ki67 labeling in the DZ at 72 h in the 1.5 mJ/mm^3 impact group.

3.2. Effects of low-energy impacts on Sox9 and progenitor cell populations

In the SZ at two hours we found significantly increased ($p = 0.0433$) labeling of Sox9 in the 3.2 mJ/mm^3 impact group compared to the 1.5 mJ/mm^3 impact group. We also found significant differences at 48 h ($p = 0.0029$) and 72 h ($p = 0.0223$) post impact.

At 24 h labeling of Sox9 decreased in the 1.5 mJ/mm^3 impact group, while this increased in the 3.2 mJ/mm^3 impact group. At 48 h we only found marginally significantly increased ($p = 0.0958$) labeling of Sox9 in the DZ of the 3.2 mJ/mm^3 impact group. At 72 h we found that this trend flipped such that we found increased labeling of Sox9 in the 1.5 mJ/mm^3 impact group compared to the 3.2 mJ/mm^3 impact group.

3.3. Effects of low-energy impacts on pEGFR and signaling pathways

In the SZ we found a greater ($p = 0.0619$) activation of pEGFR in the 3.2 mJ/mm^3 impact group compared to the 1.5 mJ/mm^3 impact group, but only at two hours post impact. At 24 h in the MZ we found marginally greater ($p = 0.0822$) activation of pEGFR. We found no difference in activation of pEGFR in the deep zone.

3.4. Linear regressions as predictors of cell labeling

We created linear regressions fitting the probability of percent positive labeling with respect to our mechanical impacts for all statistically significant differences from Table 1. In Figs. 3, 4, and 5 we summarize the linear regressions with 95% confidence intervals where we found statistically significant differences ($p < 0.05$), and marginally statistically significant differences ($0.05 \leq p < 0.10$) between the 1.5 and 3.2 mJ/mm^3 impact treatment groups.

The key differences among Figs. 3–5 are the total number of statistically significant linear regressions quantifying the relationships between the independent variable (engineering strain, first P–K stress, and impact energy density) and the dependent variable (percent positive Ki67, Sox9, and pEGFR cells). We found that several of the marginally significant differences between the 1.5 mJ/mm^3 and 3.2 mJ/mm^3 impact groups did not produce strong/significant linear regressions, see Table 2.

We found that impact energy density was the most consistent predictor of percent positive cells, with nine strong correlations spanning both multiple through-thickness zones and multiple time points post impact. We found six and five strong correlations using engineering strain or first P–K stress as the independent variable, respectively.

4. Discussion

In this study, we investigated the zone-specific cellular responses to two different levels of low-energy impact applied to articular cartilage. Our assessments of the through-thickness zones based on the morphology of chondrocytes in mature bovine cartilage generated results similar to those in human cartilage (Buckwalter et al., 1994; Athanasiou et al., 2009). Previously, we found that low-energy impacts induce micron-scale cracks in the network of collagen in articular cartilage, particularly in the SZ (Kaleem et al., 2017). Matrix repair and regulation after mechanical trauma depends on the chondrocytes (Aigner et al., 2007), however their ability to synthesize new matrix and produce more cells is extremely limited (Mankin, 1982). At

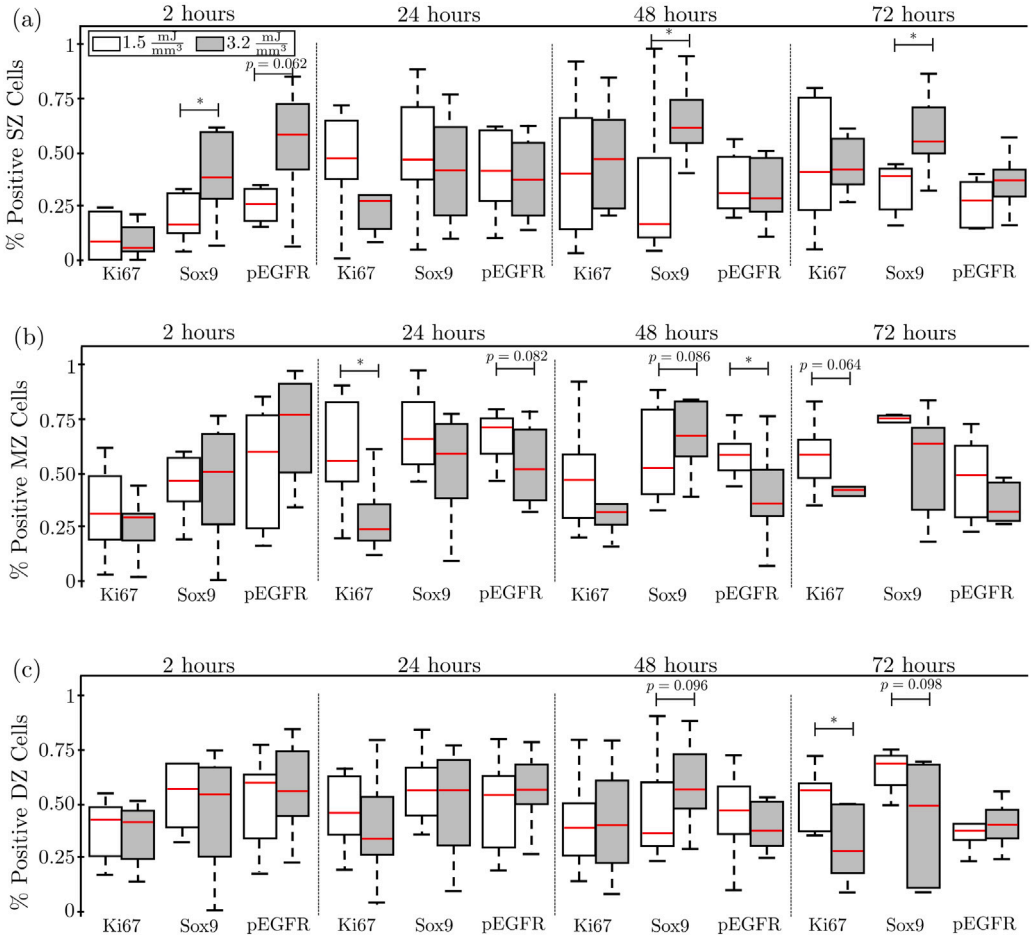

Fig. 2. Percent positive cells by through-thickness zone. We found significant differences between the 1.5 mJ/mm^3 and 3.2 mJ/mm^3 impact groups occurred in all zones, with longitudinal differences in zonal activity. Longitudinal distributions of percent positive cell labeling for Ki67, Sox9, and pEGFR after both 1.5 mJ/mm^3 and 3.2 mJ/mm^3 impacts within the (a) superficial zone (SZ), (b) middle zone (MZ), and (c) deep zone (DZ). Here * indicates differences with statistical significance ($p < 0.05$) and p-values indicate differences with marginal statistical significance ($0.05 < p < 0.10$).

least three factors may drive the cascade of degeneration that leads to post-traumatic osteoarthritis: (1) a diminished ability of chondrocytes to repair cartilage matrix (Aigner et al., 2007), (2) an increase in joint fluid adumbrates chondrocytes' repair efforts (Buckwalter et al., 1994), and (3) an insufficient number of chondrogenic progenitor cells present (Candela et al., 2014).

To test chondrocyte viability in our treatment conditions we tested the immunolocalization of C3 protein, a sensitive indicator of apoptotic cell death, in several preliminary test sections. We found negligible positive cells, present only on the surface of both unloaded and loaded explants after 72 h of *in vitro* culture (see Digital Appendix). Thus we concluded that our low-energy impacts did not cause appreciable cell death, consistent with the literature (where appreciable cell death occurred at impact energies 3 – 10× greater (Duda et al., 2001; Martin et al., 2009; Szczodry et al., 2009) and at first P–K stresses 6 – 800× greater (Duda et al., 2001; Jeffrey et al., 1995; Ewers et al., 2001) than those here).

We also aimed to determine whether measures of strain, stress, or impact energy density could predict the cellular responses. Impact loads may stimulate mechanotransduction in chondrocytes in native cartilage, including changes in gene expression (Seol et al., 2012; Novakofski et al., 2015) and signaling patterns (Rosenzweig et al., 2012). Chondrocytes encapsulated within tissue-engineered constructs present similar effects under (dynamic) cyclic compression (Salinas et al., 2019; Jeon et al., 2012, 2013). This study is the first to demonstrate altered protein levels of intra-cellular Sox9 and activation of pEGFR in chondrocytes following low-energy impact loading. We found this non-injurious mechanical stimuli altered mechanotransductive responses and that the specific responses depended on the level of load. We used 1.5 and 2.5 mJ/mm^3 as non-injurious, low-energy impacts that have ~25% and ~40% probability of microcracking the network of collagen (Kaleem et al., 2017). These impact energy densities are also below the threshold that induces cell death, which may be as low as 2 – 5 mJ/mm^3 (Duda et al., 2001). We identified ranges of mechanical inputs for up-regulation of Sox9, a chondroprogenitor cell marker, activating EGFR signaling (as indicated by pEGFR labeling), as well as proliferation, as identified by Ki67. We also determined that impact energy density was a better predictor of cell responses than measures of strain or stress.

4.1. Effects of low-energy impacts on Ki67 and cell proliferation

We found that low-energy impacts stimulated proliferation by chondrocytes in articular cartilage at least 24 h post-impact. We found no detectable difference in the amount of proliferation in the SZ. Rather, the significant differences in cell proliferation between impact groups occurred in the MZ, and marginally in the DZ. We found evidence that thresholds may exist, seen as a shift from anabolic to catabolic activity between 1.5 and 3.2 mJ/mm^3. This may suggest targets for controlled, load-informed rehabilitation for post-traumatic OA.

However, Ki67 may not indicate cell division or an increase in cell number. Rather, Ki67 is a proliferation marker that is expressed during all active phases of the cell cycle (Scholzen and Gerdes, 2000), and may

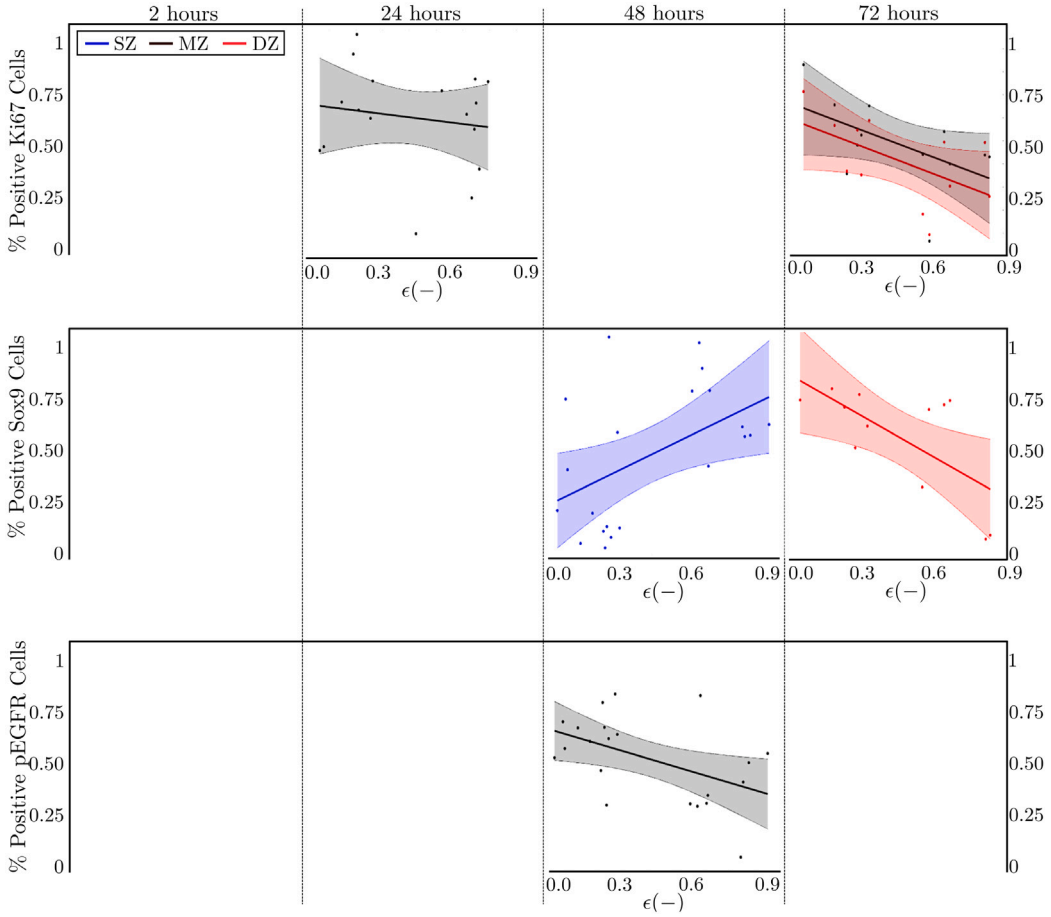

Fig. 3. Linear regressions for engineering strain. We found that engineering strain was not a consistent predictor of percent positive cell labeling, but better than first P–K stress. Summary of linear regressions for engineering strain ϵ (with 95% confidence intervals) where we found statistically significant differences ($p < 0.05$) and marginally statistically significant differences ($0.05 \leq p < 0.10$) between the 1.5 mJ/mm^3 and 3.2 mJ/mm^3 impact groups. We summarize the corresponding p-values, equations, and R^2 values in Table 2.

not predict actual cell division. We did not find significant increases in the total number of cells present in the tissue, thus low-energy impact loading may not cause a significant increase in the total number of chondrocytes (at least for time courses up to 72 h after impact). However, we did not investigate cell viability and thus changes in total cell count could be masked by flux in proliferating cells and necrotic cells. Static compression (Ryan et al., 2009) and cyclic loading (He et al., 2016) may have greater influences on cell proliferation and division than the single impact loads used in our experiments.

4.2. Effects of low-energy impacts on Sox9 and progenitor cell populations

Sox9 is an important transcription factor that serves as a master regulator of cartilage formation and differentiation (Bi et al., 1999; Lefebvre and Dvir-Ginzberg, 2017). It also maintains cartilage health by further recruiting transcriptional co-activators, histone-modifying enzymes, and other essential cellular subunits (Akiyama and Lefebvre, 2011). Both chondroprogenitors (Shepard et al., 2013) and mature (adult) chondrocytes (Fitzgerald et al., 2004; Lee et al., 2005) express the "master chondrogenic regulatory factor" Sox9 (Shepard et al., 2013) until hypertrophy (Lefebvre and Dvir-Ginzberg, 2017). Sox9 also helps regulate osteogenic differentiation and loss of cartilage phenotype, and both are catabolic activities (Liao et al., 2014). However, loss of Sox9 in articular cartilage leads to upregulation of catabolic and degradative pathways and shuts down new matrix synthesis at the transcriptional level (Henry et al., 2012). Given the well-established key roles of Sox9, we interpret positive Sox9 labeling as indication of changes in chondrocyte potential and/or functions that align with the aforementioned anabolic activities. Conversely, metabolically inactive or hypertrophic chondrocytes cannot express Sox9 (Zhao et al., 1997).

4.2.1. Temporal differences

Our results show that Sox9 labeling is highly sensitive to mechanical loading, and perhaps increased impact energy density further stimulates the master transcription factor Sox9. In the SZ we found increased impact energy density correlated with increased Sox9 labeling. Thus, if a catabolic threshold exists in the SZ it is beyond 3.2 mJ/mm^3.

No studies in the cartilage literature probe Sox9 with treatments comparable to our mechanical impact model. Multiple studies confirm transient expressions of Sox9 under compression loading (Fitzgerald et al., 2004), including after single 20–25 MPa injurious compressions (at least ten times greater than the maximum second P–K stresses in our experimental model) (Lee et al., 2005; McCulloch et al., 2014). tChan2005a found 30 MPa injurious compression repressed expression of cell adhesion molecules three hours post-injury, which can influence processes such as chondrogenic differentiation. However, we achieved maximum loads in less than 20 ms with our custom drop tower while these studies applied loads over longer periods of time. Differences in the duration of loading make direct comparisons among these experiments difficult. Since we found increased Sox9 expression, it is likely our low-energy impact loads did not repress cell adhesion molecules.

4.2.2. Zonal differences

In healthy human cartilage the percentage of Sox9 labeling increases from the SZ to the DZ (Fukui et al., 2008). We found similar trends at two hours in the 1.5 mJ/mm^3 post-impact group. Microcracks

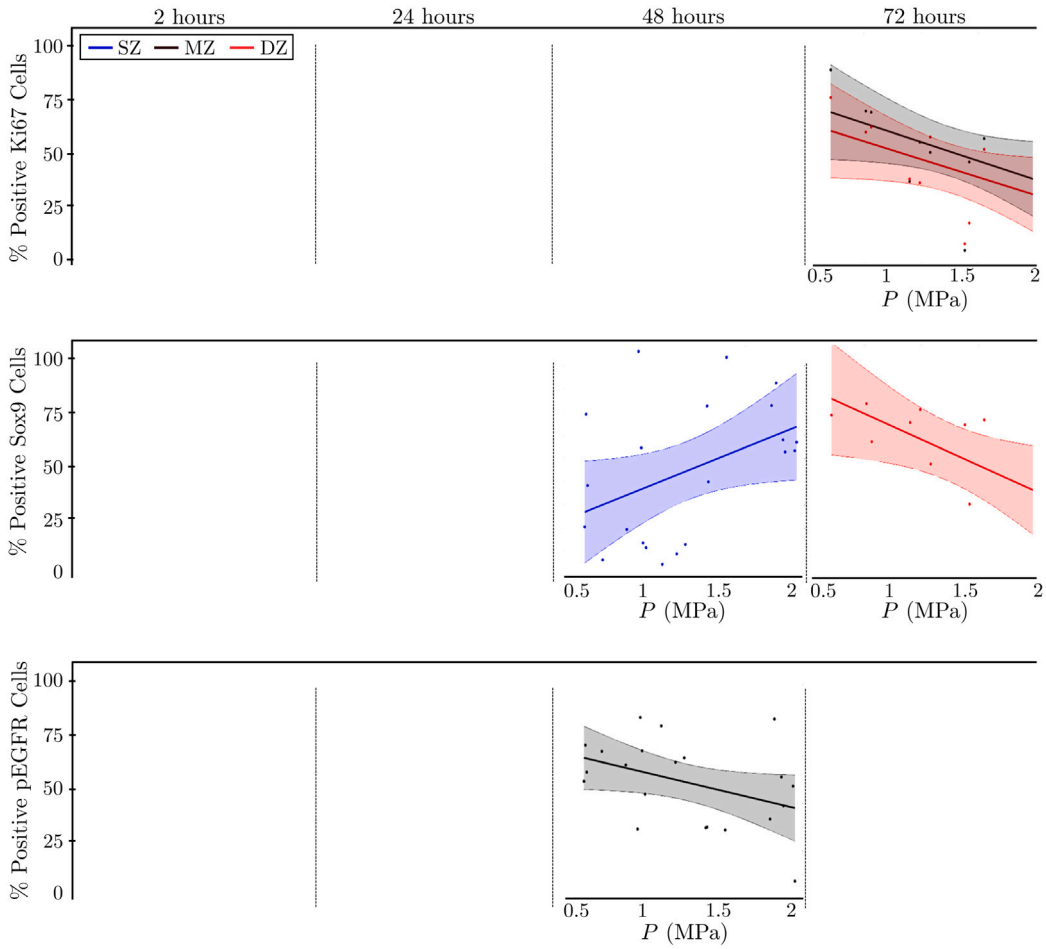

Fig. 4. Linear Regressions for first P–K stress. We found that first P–K stress was not a consistent predictor of percent positive cell labeling. Summary of linear regressions for first P–K stress P (with 95% confidence intervals) where we found statistically significant differences ($p < 0.05$) and marginally statistically significant differences ($0.05 \leq p < 0.10$) between the 1.5 mJ/mm^3 and 3.2 mJ/mm^3 impact groups. We summarize the corresponding p-values, equations, and R^2 values in Table 2.

initiate in the SZ in the same range of impact energy densities used in this study, and typically extend from the SZ into the MZ (Santos et al., 2019). Immediately after impact, we saw significantly greater Sox9 labeling in the SZ of the 3.2 mJ/mm^3 impact group, then a delayed increase to Sox9 labeling parity by the 1.5 mJ/mm^3 impact group at 24 h post impact. After 24 h, we saw significantly greater Sox9 labeling in the 3.2 mJ/mm^3 impact group in the SZ. At 3.2 mJ/mm^3 microcracks initiate in the network of collagen with a 1.6× greater probability than that at 1.5 mJ/mm^3 (Kaleem et al., 2017).

4.2.3. Chondroprogenitor activity

Due to its avascular nature cartilage may contain a large proportion of chondroprogenitor cells that may be identified using Sox9 (Grogan et al., 2009). Chondroprogenitors may be found in all three through-thickness zones, but they concentrate primarily in the two most upper zones (Grogan et al., 2009). Overall, we found greater percentages of Sox9 labeling in the MZ than the others, but more significant increases in Sox9 labeling in the SZ with increased impact energy density. This may indicate progenitor cell migration from the MZ to the SZ as a result of increased loading at the articular surface. Studies show regional chondroprogenitors migrate towards the impact site after ~70 mJ/mm^3 blunt impact (Seol et al., 2012) (> 45× our impact loads) and after ~8 mJ/mm^3 (Riegger et al., 2018) (3 – 5× greater than our impact loads). Additionally, chondroprogenitors may cluster at the articular surface, highlighting their involvement in potential matrix remodeling as a result of loading or damage (Grogan et al., 2009)

4.3. Effects of low-energy impacts on pEGFR and signaling pathways

EGFR is a tyrosine kinase receptor with multiple roles in development, homeostasis, and disease (Scaltriti and Baselga, 2006). EGFR signals regulate cartilage development and growth (Zhang et al., 2013), and EGFR activation triggers both anabolic and catabolic tissue responses (Shepard et al., 2013; Jia et al., 2016; Bellini et al., 2017). Hence joint health likely requires a balance of EGFR signals for maintenance. In healthy cartilage pEGFR labeling indicates activation of the EGFR signaling pathway (Shepard et al., 2013), and presents in all three zones. In OA-like cartilage this antibody presents only in the SZ (Jia et al., 2016). Our pEGFR labeling occurred in only the SZ and MZ, which may indicate the overall health of the tissue after loading.

We did not find simultaneous increases in both pEGFR and Ki67 labeling at the same timepoint and zone, except for at 24 h post-impact in the MZ. Thus, under our loading conditions, EGFR activation (as indicated by pEGFR labeling) via impact loading did not mediate cell proliferation. It is possible that inhibiting the EGFR signaling pathway may cause an increase in cell proliferation (He et al., 2016), though this is beyond the scope of our study. Additionally, increases in Sox9, which we saw at two hours post-impact in the SZ, may lead to changes in signaling pathway mediators (Lefebvre and Dvir-Ginzberg, 2017). This was the only time point where we saw significant differences between our loading groups in Sox9 labeling and pEGFR labeling in the same zone.

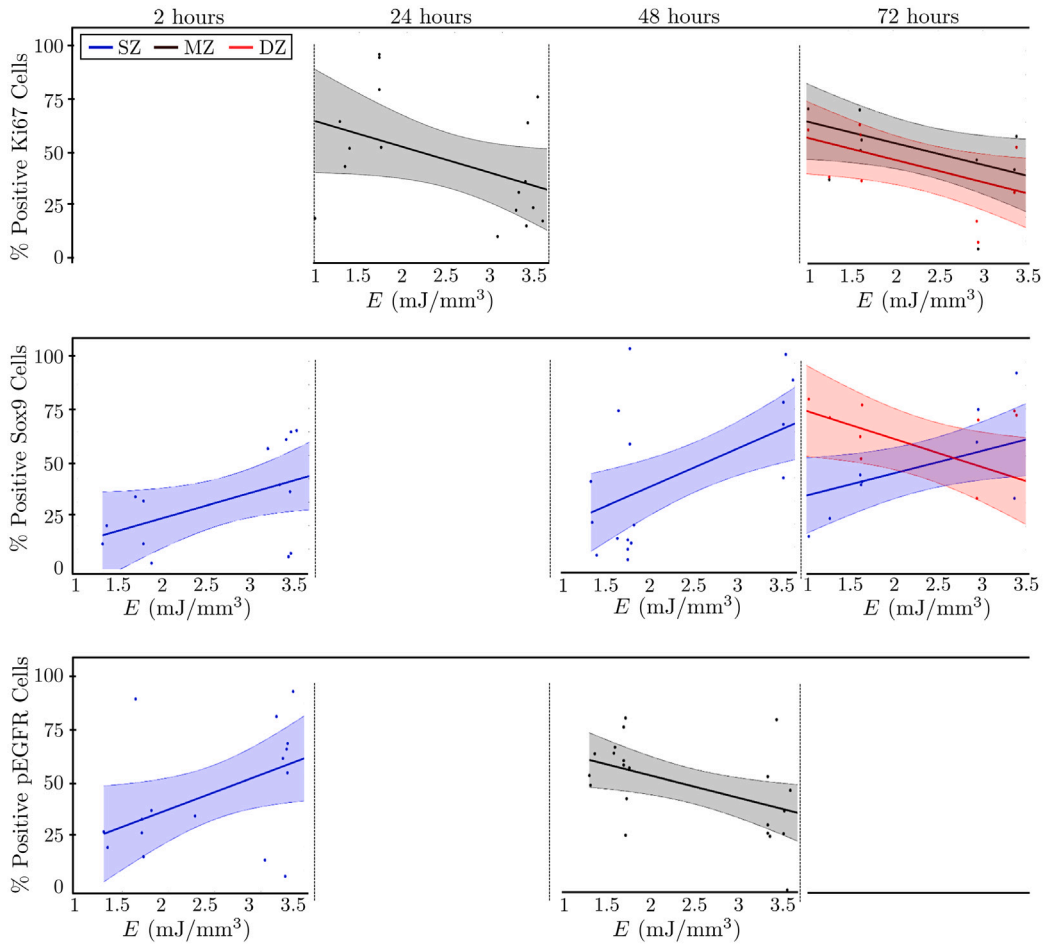

Fig. 5. Linear regressions for impact energy density. We found that impact energy density was the most consistent predictor of cell responses in proliferation, labeling, and pEGFR activation compared against both engineering strain and first P–K stress. Summary of linear regressions for impact energy density E (with 95% confidence intervals) where we found statistically significant differences ($p < 0.05$) and marginally statistically significant differences ($0.05 \leq p < 0.10$) between the 1.5 mJ/mm^3 and 3.2 mJ/mm^3 impact groups. We summarize the corresponding p-values, equations, and R^2 values in Table 2.

4.4. Linear regressions as predictors of cell labeling

Using linear regressions, we found impact energy density to be the most consistent predictor of percent positive cell responses, having the greatest number of statistically significant fits (nine) across all time points. Measures of strain relate only to deformations while measures of stress relate only to forces. Energy density, however, combines measures of both deformation and force. This may be why engineering strain and first P–K stress showed less predictive power than impact energy density. Su et al. (2018) and Kaleem et al. (2017) also found impact energy density to be a significant predictor of articular cartilage response, where Kaleem et al. (2017) found impact energy density to predict the occurrence of microcracks in the network of collagen within cartilage better than measures of strain or stress. These studies both quantified micro-mechanical damage to cartilage, not chondrocyte responses to loading. Some studies looked at genetic markers as predictors of chondrogenic differentiation (Giovannini et al., 2010; Kanawa et al., 2018), but none look at chondrocyte responses due to mechanical loading, such as chondroprogenitor cell activity and EGFR signaling or pEGFR labeling.

4.5. Limitations and outlook

Although we did not perform live/dead cell viability assays during our experiments, our preliminary results investigating C3 protein after low-energy impacts indicated negligible cell death. We assume our extraction method (using cylindrical punches to extract cylindrical plugs) caused minor structural damage at the edges of the specimens. Thus we did not analyze images near to the vertical edges of the specimens. To determine through-thickness boundaries parallel to the articular surface for each zone during image analysis, we manually determined transitions based changes in cellular shape and arrangement. We attempted to minimize human-bias by selecting boundaries in the middle of transition zones. We also experienced minor discrepancies with our immunohistochemical staining likely due to environmental conditions and human factors. Finally, we recognize that our study used only two impact energy densities. Future studies could incorporate additional impact energy densities to better elucidate the relationship between impact energy density and percent positive cells.

Our study demonstrates that low-energy mechanical impacts (1.5–3.2 mJ/mm^3) generally stimulate time-dependent anabolic responses in the superficial zone of articular cartilage and catabolic responses in the middle and deep zones. We also found that impact energy density is the most consistent predictor of cell responses to low-energy impact loading. These spatial and temporal changes in chondrocyte behaviors result directly from low-energy mechanical impacts, revealing a new level of mechanotransductive sensitivity in chondrocytes not previously appreciated. Understanding subtle changes in chondrocyte behaviors under low-energy mechanical impacts may provide (1) better insight on the initiation of regeneration/degeneration in cartilage and (2) improved targets for the development of person-made cartilage substitutes, i.e. zonal tissue engineering. Finally, our data may

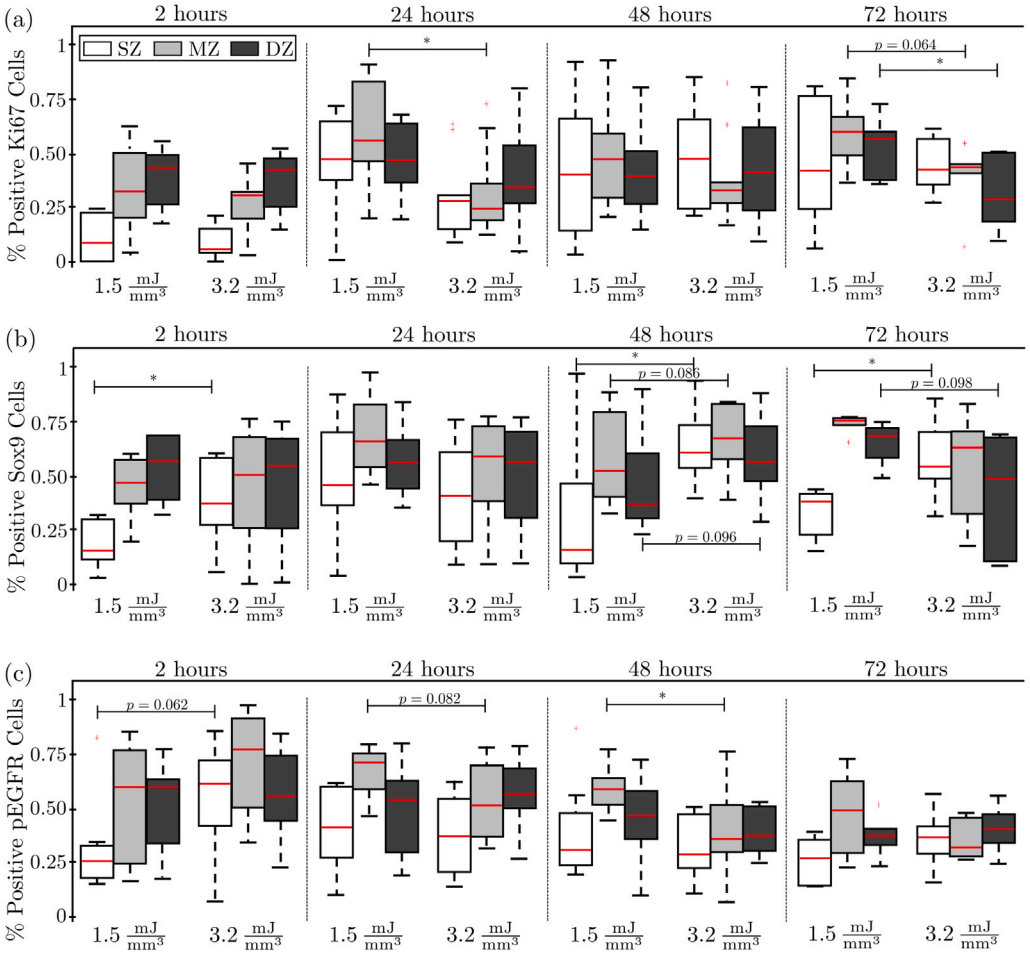

Fig. 6. Percent positive cells by antibody. We found significant differences between the 1.5 mJ/mm^3 and 3.2 mJ/mm^3 impact groups occurred in all zones, with longitudinal differences in zonal activity. Longitudinal distributions of percent positive cell labeling within the superficial zone (SZ), middle zone (MZ), and deep zone (DZ) after both 1.5 mJ/mm^3 and 3.2 mJ/mm^3 impacts for (a) Ki67, (b) Sox9, and (c) pEGFR. Here * indicates differences with statistical significance ($p < 0.05$) and p-values indicate differences with marginal statistical significance ($0.05 < p < 0.10$).

aid in developing and calibrating predictive computational models of remodeling or damage in both cartilage and joints.

Funding

The National Science Foundation and the Ford Fellowship Foundation had no involvement in the study design; in collection, analysis and interpretation of data; in the writing of the manuscript; or in the decision to submit the manuscript for publication. Any opinions, findings, and conclusions or recommendations expressed in this material are those of the author(s) and do not necessarily reflect the views of the National Science Foundation.

CRediT authorship contribution statement

Stephany Santos: Conceptualization, Data curation, Formal analysis, Investigation, Methodology, Software, Validation, Visualization, Writing - original draft, Writing - review & editing. **Kelsey Richard:** Conceptualization, Data curation, Formal analysis, Investigation, Methodology, Software, Validation, Visualization, Writing - original draft, Writing - review & editing. **Melanie C. Fisher:** Conceptualization, Methodology, Supervision, Writing - original draft. **Caroline N. Dealy:** Conceptualization, Formal analysis, Funding acquisition, Methodology, Project administration, Resources, Supervision, Validation, Writing - original draft, Writing - review & editing. **David M. Pierce:** Conceptualization, Data curation, Formal analysis, Funding acquisition, Investigation, Methodology, Project administration, Resources, Software, Supervision, Validation, Visualization, Writing - original draft, Writing - review & editing.

Declaration of competing interest

The authors declare that they have no known competing financial interests or personal relationships that could have appeared to influence the work reported in this paper.

Acknowledgments

We gratefully acknowledge funding from the National Science Foundation, USA (CAREER and standard) 1653358, NSF 1662429, and the Ford Fellowship Foundation. We thank Caitlyn Monterosso for assistance processing and staining specimens. We thank Sara Anwer, Avery Carroll, Dalia Clarke, Andreya Gardener, Alyssa Harvey, Hermana Henry, Millenia Polanco, Amanda Reid, Bryanna Samolyk, Faith Sporbert, and Brianna Westenfield for assistance analyzing images and organizing data. We also thank Dr. James Grady and Rong Wu from the Connecticut Institute for Clinical and Translational Science for consulting on statistics.

Appendix A

In Fig. 6 we quantified immuno-labeling (the localization of each antibody) by antibody and time post impact.

Table 2
Impact energy density (E) and engineering strain (ϵ) are better predictors of percent positive cell labeling than first P–K stress (P). Summary of equations for linear regressions by antibody (Ki76, Sox9, and pEGFR), through-thickness zone (superficial zone (SZ), middle zone (MZ), and deep zone (DZ)), and time post impact (2, 24, 48, and 72 h). We indicate statistical significance ($p < 0.05$) with * and dark gray shading, and marginal statistical significance ($0.05 \leq p < 0.10$) with light gray shading.

Antibody	Zone	Time	p	Equation	R^2
Ki67	MZ	24 h	**0.043***	$-0.604\epsilon + 0.716$	0.243
			0.150	–	–
			0.029*	$-0.121E + 0.710$	0.279
		72 h	**0.054**	$-0.471\epsilon + 0.722$	0.322
			0.055	$-0.160P + 0.685$	0.320
			0.054	$-0.093E + 0.700$	0.322
	DZ	72 h	**0.062**	$-0.451\epsilon + 0.642$	0.302
			0.064	$-0.152P + 0.605$	0.303
			0.042*	$-0.095E + 0.634$	0.352
Sox9	SZ	2 h	0.290	–	–
			0.143	–	–
			0.055	$0.116E + 0.009$	0.256
		48 h	**0.040***	$0.565\epsilon + 0.203$	0.204
			0.052	$0.221P + 0.230$	0.184
			0.024*	$0.119E + 0.201$	0.240
		72 h	0.108	–	–
			0.244	–	–
			0.048*	$0.097E + 0.232$	0.337
	MZ	48 h	0.105	–	–
			0.225	–	–
			0.106	–	–
	DZ	48 h	0.153	–	–
			0.277	–	–
			0.166	–	–
		72 h	**0.016***	$-0.694\epsilon + 0.886$	0.455
			0.032*	$-0.217P + 0.808$	0.384
			0.040*	$-0.121E + 0.815$	0.357
pEGFR	SZ	2 h	0.381	–	–
			0.409	–	–
			0.098	$0.118E + 0.164$	0.161
	MZ	24 h	0.205	–	–
			0.245	–	–
			0.247	–	–
		48 h	**0.049***	$-0.328\epsilon + 0.632$	0.189
			0.064	$-0.123P + 0.615$	0.169
			0.042*	$-0.065E + 0.626$	0.200

Appendix B. Supplementary data

Supplementary material related to this article can be found online at https://doi.org/10.1016/j.jmbbm.2020.104252.

References

Aigner, T., Söder, S., Gebhard, P., McAlinden, A., Haag, J., 2007. Mechanisms of disease: Role of chondrocytes in the pathogenesis of osteoarthritis- structure, chaos and senescence. Nat. Clin. Pract. Rheum. 3, 391–399.

Akiyama, H., Lefebvre, V., 2011. Unraveling the transcriptional regulatory machinery in chondrogenesis. J. Bone Miner. Metab. 29, 390–395.

Anderson, D.D., Chubinskaya, S., Guilak, F., Martin, J.A., Oegema, T., Olson, S.A., et al., 2011. Post-traumatic osteoarthritis: improved understanding and opportunities for early intervention. J. Orthop. Res. 29 (6), 802–809.

Athanasiou, K.A., Darling, E.M., Hu, J.C., 2009. Articular Cartilage Tissue Engineering: Synthesis Lectures on Tissue Engineering. Morgan & Claypool Publishers, San Rafael, CA.

Bellini, M., Pest, M., Beier, F., 2017. EGFR/MIG-6 signalling in osteoarthritis. Osteoarthr. Cartil. 25 (2017), S143–S144.

Bi, W., Deng, J.M., Zhang, Z., Behringer, R.R., Crombrugghe, B.D., 1999. Sox9 is required for cartilage formation. Nat. Genet. 22, 85–89.

Buckwalter, J.A., Mow, V.C., Ratcliffe, A., 1994. Restoration of injured or degenerated articular cartilage. J. Am. Acad. Orthop. Surg. 2, 192–201.

Candela, M.E., Yasuhara, R., Iwamoto, M., Enomoto-Iwamoto, M., 2014. Resident mesenchymal progenitors of articular cartilage. Matrix Biol. 39, 44–49.

Chan, P.S., Schlueter, A.E., Coussens, P.M., Rosa, G.J., Haut, R.C., Orth, M.W., 2005. Gene expression profile of mechanically impacted bovine articular cartilage explants. J. Orthop. Res. 23 (5), 1146–1151.

Chen, S.S., Falcovitz, Y.H., Schneiderman, R., Maroudas, a., Sah, R.L., 2001. Depth-dependent compressive properties of normal aged human femoral head articular cartilage: Relationship to fixed charge density. Osteoarthr. Cartil. 9 (6), 561–569.

Duda, G.N., Eilers, M., Loh, L., Hoffman, J.E., Kääb, M., Schaser, K., 2001. Chondrocyte death precedes structural damage in blunt impact trauma. Clin. Orthop. Relat. Res. 393, 302–309.

Ewers, B.J., Dvoracek-Driksna, D., Orth, M.W., Haut, R.C., 2001. The extent of matrix damage and chondrocyte death in mechanically traumatized articular cartilage explants depends on rate of loading. J. Orthop. Res. 19, 779–784.

Fitzgerald, J.B., Jin, M., Dean, D., Wood, D.J., Zheng, M.H., Grodzinsky, A.J., 2004. Mechanical compression of cartilage explants induces multiple time-dependent gene expression patterns and involves intracellular calcium and cyclic AMP. J. Bio. Chem. 279 (19), 19502–19511.

Fukui, N., Ikeda, Y., Ohnuki, T., Tanaka, N., Hikita, A., Mitomi, H., et al., 2008. Regional differences in chondrocyte metabolism in osteoarthritis: A detailed analysis by laser capture microdissection. Arthritis Rheum. 58 (1), 154–163.

Giovannini, S., Diaz-Romero, J., Aigner, T., Mainil-Varlet, P., Nesic, D., 2010. Population doublings and percentage of S100-positive cells as predictors of in vitro chondrogenicity of expanded human articular chondrocytes. J. Cell Physiol. 222 (2), 411–420.

Grogan, S.P., Miyaki, S., Asahara, H., D'Lima, D.D., Lotz, M.K., 2009. Mesenchymal progenitor cell markers in human articular cartilage: Normal distribution and changes in osteoarthritis. Arthritis Res. Ther. 11 (3), 1–13.

He, P., Shen, N., Gao, G., Jiang, X., Sun, H., Zhou, D., et al., 2016. Periodic mechanical stress activates PKCδ-dependent EGFR mitogenic signals in rat chondrocytes via PI3K-Akt and ERK1/2. Cell. Physiol. Biochem. 39, 1281–1294.

Henry, S.P., Liang, S., Akdemir, K.C., De Crombrugghe, B., 2012. The postnatal role of Sox9 in cartilage. J. Bone Miner. Res. 27 (12), 2511–2525.

Jeffrey, J., Gregory, D.W., Aspden, R.M., 1995. Matrix damage and chondrocyte viability following a single impact load on articular cartilage. Arch. Biochem. Biophys. 322, 87–96.

Jeon, J.E., Schrobback, K., Hutmacher, D.W., Klein, T.J., 2012. Dynamic compression improves biosynthesis of human zonal chondrocytes from osteoarthritis patients. Osteoarthr. Cartil. 20 (8), 906–915. http://dx.doi.org/10.1016/j.joca.2012.04.019.

Jeon, J.E., Schrobback, K., Meinert, C., Sramek, V., Hutmacher, D.W., Klein, T.J., 2013. Effect of preculture and loading on expression of matrix molecules, matrix metalloproteinases, and cytokines by expanded osteoarthritic chondrocytes. Arthritis Rheum. 65 (9), 2356–2367.

Jia, H., Ma, X., Tong, W., Doyran, B., Sun, Z., Wang, L., et al., 2016. EGFR Signaling is critical for maintaining the superficial layer of articular cartilage and preventing osteoarthritis initiation. Proc. Acad. Sci. USA 113 (50), 14360–14365.

Kaleem, B., Maier, F., Drissi, H., Pierce, D., 2017. Low-energy impact of human cartilage: Predictors for microfracturing the network of collagen. Osteoarthr. Cartil 25, 544–553.

Kamekura, S., Hoshi, K., Shimoaka, T., Chung, U., Chikuda, H., Yamada, T., et al., 2005. Osteoarthritis development in novel experimental mouse models induced by knee joint instability. Osteoarthr. Cartil. 13 (7), 632–641.

Kanawa, M., Igarashi, A., Fujimoto, K., Higashi, Y., Kurihara, H., Sugiyama, M., et al., 2018. Genetic markers can predict chondrogenic differentiation potential in bone marrow-derived mesenchymal stromal cells. Stem Cells Int 2018, 1–9.

Lahm, A., Mrosek, E., Spank, H., Erggelet, C., Kasch, R., Esser, J., et al., 2010. Changes in content and synthesis of collagen types and proteoglycans in osteoarthritis of the knee joint and comparison of quantitative analysis with photoshop-based image analysis. Arch. Orthop. Trauma Surg. 130 (4), 557–564.

Lee, J.H., Fitzgerald, J.B., DiMicco, M.A., Grodzinsky, A.J., 2005. Mechanical injury of cartilage explants causes specific time-dependent changes in chondrocyte gene expression. Arthritis Rheum. 52, 2386–2395.

Lefebvre, V., Dvir-Ginzberg, M., 2017. SOX9 and the many facets of its regulation in the chondrocyte lineage. Connect Tissue Res. 58 (1), 2–14.

Liao, J., Hu, N., Zhou, N., Lin, L., Zhao, C., Yi, S., et al., 2014. Sox9 potentiates BMP2-induced chondrogenic differentiation and inhibits BMP2-induced osteogenic differentiation. PLoS One 9, e89025.

Mankin, H., 1982. The response of articular cartilage to mechanical injury. J. Bone Joint Surg. Am. 64, 460–466.

Martin, J.A., McCabe, D., Walter, M., Buckwalter, J.A., McKinley, T.O., 2009. N-acetylcysteine inhibits post-impact chondrocyte death in osteochondral explants. J. Bone Joint Surg. 91 (8), 1890–1897.

McCulloch, R.S., Ashwell, M.S., Maltecca, C., O'Nan, A.T., Mente, P.L., 2014. Progression of gene expression changes following a mechanical injury to articular cartilage as a model of early stage osteoarthritis. Arthritis 2014, 1–9.

Novakofski, K.D., Berg, L.C., Bronzini, I., Bonnevie, E.D., Poland, S.G., Bonassar, L.J., et al., 2015. Joint-dependent response to impact and implications for post-traumatic osteoarthritis. Osteoarthr. Cartil. 23, 1130–1137.

Pedersen, D.R., Goetz, J.E., Kurriger, G.L., Martin, J.A., 2013. Comparative digital cartilage histology for human and common osteoarthritis models. Orthop. Res. Rev. 2013, 13–20.

Perera, P.M., Wypasek, E., Madhavan, S., Rath-Deschner, B., Liu, J., Nam, J., et al., 2010. Mechanical signals control SOX-9, VEGF, and c-myc expression and cell proliferation during inflammation via integrin-linked kinase, B-raf, and ERK1/2-dependent signaling in articular chondrocytes. Arthritis Res. Ther. 12 (3), 1–9.

Preibisch, S., Saalfeld, S., Tomancak, P., 2009. Globally optimal stitching of tiled 3D microscopic image acquisitions. Bioinformatics 25, 1463–1465.

Riegger, J., Palm, H., Brenner, R., 2018. The functional role of chondrogenic stem/progenitor cells: novel evidence for immunomodulatory properties and regenerative potential after cartilage injury. Eur. Cell Mater. 36, 110–127.

Rosenzweig, D.H., Djap, M.J., Ou, S.J., Quinn, T.M., 2012. Mechanical injury of bovine cartilage explants induces depth-dependent, transient changes in MAP kinase activity associated with apoptosis. Osteoarthr. Cartil. 20, 1591–1602.

Ryan, J.A., Eisner, E.A., DuRaine, G., You, Z., Reddi, A.H., 2009. Mechanical compression of articular cartilage induces chondrocyte proliferation and inhibits proteoglycan synthesis by activation of the ERK pathway: implications for tissue engineering and regenerative medicine. J. Tissue Eng. Regen. Med. 3, 107–116.

Saha, A.K., Kohles, S.S., 2010. A distinct catabolic to anabolic threshold due to single-cell static nanomechanical stimulation in a cartilage biokinetics model. J. Nanotechnol. Eng. Med. 1 (3), 1–8.

Salinas, D., Mumey, B.M., June, R.K., 2019. Physiological dynamic compression regulates central energy metabolism in primary human chondrocytes. Biomech. Model. Mechanobiol. 18 (1), 69–77. http://dx.doi.org/10.1007/s10237-018-1068-x.

Santos, S., Emery, N., Neu, C.P., Pierce, D.M., 2019. Propagation of microcracks in collagen networks of cartilage under mechanical loads. Osteoarthr. Cartil. 27, 1392–1402.

Scaltriti, M., Baselga, J., 2006. The epidermal growth factor receptor pathway a model for targeted therapy. Clin. Cancer Res. 12, 5268–5272.

Scholzen, T., Gerdes, J., 2000. The Ki-67 protein: From the known and the unknown. J. Cell Physiol. 182, 311–322.

Seol, D., Mccabe, D.J., Choe, H., Zheng, H., Yu, Y., Jang, K., et al., 2012. Chondrogenic progenitor cells respond to cartilage injury. Arthritis Rheum. 64 (11), 3626–3637.

Setton, L., Mow, V.C., Howell, D.S., 1995. Mechanical behavior of articular cartilage in shear is altered by transection of the anterior cruciate ligament. J. Orthop. Res. 13, 473–482.

Shepard, J.B., Jeong, J.-W., Maihle, N.J., O'Brien, S., Dealy, C.N., 2013. Transient anabolic effects accompany epidermal growth factor receptor signal activation in articular cartilage in vivo. Arthritis Res. Ther. 15 (3), R60.

Su, A.W., Chen, Y., Dong, Y., Wailes, D.H., Wong, V.W., Chen, A.C., et al., 2018. Biomechanics of osteochondral impact with cushioning and graft insertion: Cartilage damage is correlated with delivered energy. J. Biomech. 73, 127–136.

Szczodry, M., Coyle, C.H., Kramer, S.J., Smolinski, P., Chu, C.R., 2009. Progressive chondrocyte death after impact injury indicates a need for chondroprotective therapy. Am. J. Sports Med. 37 (12), 2318–2322.

Verteramo, A., Seedhom, B.B., 2007. Effect of a single impact loading on the structure and mechanical properties of articular cartilage. J. Biomech. 40, 3580–3589.

Youn, I., Choi, J.B., Cao, L., Setton, L.A., Guilak, F., 2006. Zonal variations in the three-dimensional morphology of the chondron measured in situ using confocal microscopy. Osteoarthr. Cartil. 14 (9), 889–897.

Zhang, L., Lake, S.P., Lai, V.K., Picu, C.R., Barocas, V.H., Shephard, M.S., 2013. A coupled fiber-matrix model demonstrates highly inhomogeneous microstructural interactions in soft tissues under tensile load. J. Biomed. Eng. 135, 011008-011008-9.

Zhao, Q., Eberspaecher, H., Lefebvre, V., De Crombrugghe, B., 1997. Parallel expression of Sox9 and Col2a1 in cells undergoing chondrogenesis. Dev. Dyn. 209 (4), 377–386.